Cross sections for the formation of ^{84m,g}Rb, ^{83}Rb, and ^{82m}Rb in ^{86}Sr(d, x) reactions up to deuteron energies of 49 MeV: Competition between α-particle and multinucleon emission processes

M. S. Uddin ®,[1,2,3] S. Sudár ®,[4] M. S. Basunia ®,[2] I. Spahn ®,[1] A. S. Voyles ®,[2,5] A. Hermanne,[6] L. A. Bernstein ®,[2,5]
B. Neumaier ®,[1] and S. M. Qaim ®[1,*]

[1]*Institut für Neurowissenschaften und Medizin, INM-5: Nuklearchemie, Forschungszentrum Jülich, D-52425 Jülich, Germany*
[2]*Nuclear Science Division, Lawrence Berkeley National Laboratory, Berkeley, California 94720, USA*
[3]*Tandem Accelerator Facilities, INST, Atomic Energy Research Establishment, Savar, Dhaka, Bangladesh*
[4]*Institute of Experimental Physics, Debrecen University, H-4001 Debrecen, Hungary*
[5]*Department of Nuclear Engineering, University of California, Berkeley, Berkeley, California 94720, USA*
[6]*Cyclotron Laboratory, Vrije Universiteit Brussel (VUB), B-1090 Brussels, Belgium*

Cross sections of ^{86}Sr(d,x) reactions leading to the products ^{84m,g}Rb, ^{83}Rb, and ^{82m}Rb were measured by the stacked-sample activation technique up to deuteron energies of 49 MeV. Nuclear model calculations were performed using the codes TALYS and EMPIRE, which combine the statistical, precompound, and direct interaction components. In all cases, the EMPIRE results were much higher than the TALYS calculation. Fairly good agreement was obtained between measured data and the TALYS calculation after some optimization of the input model parameters. Insight into competition between α-particle and multinucleon emission in the ^{88}Y compound-nucleus system was also gained.

I. INTRODUCTION

Over the last 30 years, extensive experimental work has been performed in many laboratories on nuclear reactions induced by light-charged particles, mainly using the activation technique [1]. This methodology involves a quantitative assay of the radioactive product without any direct measurement of the promptly emitted radiation. The experimental data obtained are thus of integral nature but are of great practical value in optimization of production conditions of potentially useful medical radionuclides [2]. The data are also useful to a varying extent in testing nuclear models, based on the system being explored. For this purpose, however, it is advisable to perform measurement on a monoisotopic element or on an isotopically enriched target isotope, both of which restrict the number of compound nuclei formed and thus somewhat simplify the interpretation of the reaction channels, leading to the formation of the product nucleus under investigation.

Of all the light-charged particles, protons have been by far most commonly used in nuclear reaction cross-section measurements, mainly up to energies of 30 MeV, but also in some cases up to 100 MeV and beyond. The data find extensive use in production of short-lived radionuclides at small- and medium-sized cyclotrons (cf. Refs. [3–5]) for positron emission tomography (PET) as well as for single-photon emission computed tomography. Regarding reaction theory, except for the very light mass element region, the data are described fairly well by the available modern nuclear model codes, especially when the experimental database is strong. At intermediate energies, i.e., $E \geqslant 40$ MeV, however, both experimental databases and nuclear model calculations need further improvement (cf. Refs. [6–8]). In recent years, on the other hand, interest in reactions induced by other charged particles has also been increasing, especially when considering production of many emerging radionuclides [9]. The status of use of α particles has been reviewed [10]. The ^{3}He−particle beam is not commonly available. But, deuteron-induced reactions have been attracting more attention, although it is apparent that the measured activation cross sections are somewhat difficult to describe by the model calculations (cf. Refs. [11–15]).

In a recent work, we reported in detail our experimental and theoretical studies on (d,xn) reactions on highly enriched ^{86}Sr target at deuteron energies up to 49 MeV [16]. The cross-section data as well as the isomeric cross-section ratios of the $(d, 2n)$ and $(d, 3n)$ reactions leading to the formation of ^{86m,g}Y and ^{85m,g}Y, respectively, could be partially reproduced by the nuclear model calculations. The cross-section data for the (d,n) reaction products, viz., ^{87m,g}Y, however, were somewhat difficult to reproduce by the model calculation. We now extend those studies to the product radionuclides ^{84m,g}Rb, ^{83}Rb, and ^{82m}Rb, which involve emission of an α particle as well as multinucleons. The major aim was to test the applicability of the nuclear model calculations to describe the total formation cross sections of those products and to gain some information on competition between multinucleon and α-particle emission. For this purpose, several variations of the codes TALYS and EMPIRE were used. A further aim was to obtain data on new alternative production routes of the medically interesting radionuclides ^{82m}Rb and ^{83}Rb, the former for use in cardiac studies via PET (cf. Ref. [17]) and the latter for potential use in radiotherapy with Auger electrons [18].

---

*Contact author: s.m.qaim@fz-juelich.de

TABLE I. Decay data including β^+, EC branching [22–25], and production routes of the investigated radionuclides in irradiations of enriched ^{86}Sr with deuterons of energies up to 49 MeV.

Radionuclide	Spin	Decay mode (%)	Half-life	γ-ray energy (keV)	γ-ray intensity (%)	Production route	Q value (MeV)
^{82m}Rb	5^-	$\beta^+ = 21.2$ $EC = 78.8$	6.472(6) h	554.4 619.1	62.4(9) 37.98(9)	^{86}Sr$(d,2n\alpha)$ ^{87}Sr$(d,3n\alpha)$[a] ^{88}Sr$(d,4n\alpha)$[a]	-13.84 -22.26 -33.38
^{83}Rb	$5/2^-$	$EC = 100$	86.2(1) d	520.4 529.6	44.7 (33) 29.3 (21)	^{86}Sr$(d,n\alpha)$ ^{86}Sr$(d, 3n2p)$ ^{86}Sr$(d, 2n^3\text{He})$ ^{86}Sr$(d, 5n)^{83}$Y $\rightarrow$ ^{83}Sr ^{86}Sr$(d, 4np)^{83}$Sr $\rightarrow$ ^{83}Rb ^{87}Sr$(d,2n\alpha)$[a] ^{88}Sr$(d,3n\alpha)$[a]	-2.81 -31.11 -23.39 -39.54 -34.16 -11.24 -22.35
^{84m}Rb	6^-	$IT = 100$	20.26(4) min	215.6 248.0 463.6	29.5(12)[b] 60.2(8)[b] 36.1(12)[b]	^{86}Sr(d,α) ^{86}Sr$(d, 2n2p)$ ^{86}Sr(d,npd) ^{86}Sr$(d, n^3\text{He})$ ^{87}Sr$(d,n\alpha)$[a] ^{88}Sr$(d,2n\alpha)$[a]	5.48 -22.81 -20.59 -15.09 -2.95 -14.06
^{84}Rb	2^-	$\beta^+ = 26$ $EC = 70.1$ $\beta^- = 3.9$	32.82(7) d	881.6	69 (2)	^{86}Sr(d,α) ^{86}Sr$(d, 2n2p)$ ^{86}Sr(d,npd) ^{86}Sr$(d, n^3\text{He})$ ^{87}Sr$(d,n\alpha)$[a] ^{88}Sr$(d,2n\alpha)$[a]	5.95 -22.35 -20.12 -14.63 -2.48 -13.59

[a]This reaction occurs on the respective impurity target isotope present in low abundance in the enriched ^{86}Sr target.

[b]The recommended values of Ref. [22] are preferred over the values of Ref. [25] for better precision. The data of our work also supported the values of Ref. [22].

II. EXPERIMENT

A. Sample preparation, irradiation, radioactivity measurement, and deuteron flux determination

The stacked-sample activation technique was applied to measure excitation functions of deuteron-induced reactions on a series of enriched ^{86}Sr targets provided as ^{86}Sr CO$_3$ powder (isotopic composition: 96.4% ^{86}Sr; 1.33% ^{87}Sr; and 2.26% ^{88}Sr; supplied by Eurisotop, France). Thin strontium carbonate samples were prepared by the sedimentation technique at the Forschungszentrum Jülich (FZJ), Germany, the details of which have been reported elsewhere [19]. The irradiation and radioactivity measurement techniques have also been described [16,19,20]. Here, we mention only some salient features relevant to the present measurements. Two stacks of ^{86}Sr CO$_3$ samples with the Al, Ti, Fe, and Cu monitor foils and absorbers were irradiated with deuterons of primary energies 33 and 40 MeV, for 30 and 45 min, respectively, at the 88-inch Cyclotron, Lawrence Berkeley National Laboratory (LBNL), USA, at a beam current of 100 nA. Thereafter, the radioactivity measurements of all the samples irradiated at LBNL were done there. Two other stacks were irradiated with 50-MeV primary energy deuterons using the external beam of the CGR930 Cyclotron of the Université Catholique in Louvain-la-Neuve, Belgium, each for 30 min at a beam current of approximately 200 nA. Those irradiated samples were transferred by special transport to the Nuclear Chemistry Laboratory of the FZJ, about 200 km away, where γ-ray spectral measurements were carried out.

The radioactivity of a reaction product in the activated monitor foil or Sr sample was measured nondestructively using high-purity germanium γ-ray detectors associated with the necessary electronics and MAESTRO data acquisition software. The γ-ray spectrometric facilities at FZJ, Germany and LBNL, USA utilized to carry out radioactivity measurements were well calibrated for energy and efficiency using the standard point sources ^{22}Na, ^{54}Mn, ^{57}Co, ^{60}Co, ^{88}Y, ^{137}Cs, ^{152}Eu, ^{226}Ra, and ^{241}Am (supplied by Eckert & Ziegler, Berlin) at FZJ and ^{54}Mn, ^{133}Ba, ^{137}Cs, and ^{152}Eu (supplied by Isotope Products Laboratories) at LBNL. The uncertainty in the activity of each source was specified as 3%. The γ-ray spectra measured in this work were analyzed by both GAMMAVISION and FITZPEAKS [21] software. The decay data of the radionuclide ^{84m}Rb were taken from the Lund/LBNL Nuclear Database [22] and those for the other investigated radionuclides from some recent references [23–25]; they are collectively given in Table I.

At LBNL, the short-lived ^{84m}Rb ($T_{1/2} = 20.26$ min) activity was measured within 10 to 60 min after end of bombardment (EOB). To reduce the dead time, each sample was counted at a distance of 40, 50, or 60 cm, where the low efficiency disfavored the counting statistics. It was identified by its characteristic γ rays of energies 215.6, 248.0, and 463.6 keV, respectively. In the FZJ experiment, this radionu-

clide decayed out during the sample transport from Louvain-la-Neuve (Belgium) to Jülich, and so it could not be measured.

The metastable state ^{82m}Rb ($T_{1/2} = 6.472$ h) measurement was started one day after EOB at FZJ. It was done at a distance of 15 cm. Due to the high threshold for its formation, the ^{82m}Rb activity could be measured at LBNL only in a few samples.

The last step of counting was devoted to the measurement of the long-lived radionuclides ^{83}Rb ($T_{1/2} = 86.2$ d) and ^{84}Rb ($T_{1/2} = 32.82$ d) at a distance of 5 cm from the detector surface to obtain good counting statistics. The counting was started about 10–13 days after EOB and carried out for 10 to 30 h. Due to the allowed decay time, the background was drastically reduced and well-resolved peaks at energies of 520.4, 529.6, and 881.6 keV could be identified and quantified satisfactorily. The first two gamma lines are emitted in the decay of ^{83}Rb and the third one in ^{84}Rb. The radionuclide ^{83}Rb was formed directly and additionally through decay of the series of ^{83}Y ($T_{1/2} = 7.08$ min)$\rightarrow$ ^{83}Sr($T_{1/2} = 32.41$ h)$\rightarrow$ ^{83}Rb via $\beta^+ +$ EC processes. Likewise, the radionuclide ^{83}Sr was formed via the ^{86}Sr($d, 4np$) reaction and in the decay of ^{83}Y. A significant contribution from the decay of ^{83}Sr in the formation of ^{83}Rb was observed above 40-MeV deuteron beam energy. The allowed waiting time was enough for complete decay of the radionuclide ^{83}Sr to ^{83}Rb before the measurement.

Each sample was counted 3–4 times using appropriate acquisition intervals to validate the half-lives of the activation products as well as to avoid interferences by overlapping γ lines from undesired products. For all of the above counting distances, the random coincidence losses as well as the effect of the sample size on the efficiency became negligible. The correction for true coincident γ-ray summing was also negligible. At FZJ, the measurement of each sample was carried out by two separate detectors, which was useful to eliminate any bias resulting from the detector efficiency.

The method for calculation of deuteron energy degradation in the stack and the technique for its flux measurement in these irradiations via the monitor reactions ^{27}Al(d, x) ^{24}Na, ^{nat}Ti(d,x)^{48}V, ^{nat}Fe(d, x) ^{56}Co, and ^{nat}Cu(d,x)^{62,63}Zn have already been described [16]. Those same energy- and flux values were used in investigations on Rb isotopes described in this work. The cross sections for those monitor reactions were adopted from the IAEA-recommended values [26].

B. Reaction cross section and its uncertainty

The count rate of the characteristic γ ray of a radionuclide was back-extrapolated to EOB and then converted to its decay rate by applying the necessary corrections for γ-ray intensity, self-absorption, efficiency of the detector, and true coincidence losses, if any. From the decay rate at EOB and the measured deuteron beam flux, the cross section for the formation of a radionuclide was determined using the well-known activation formula.

The contributions to the reaction product from subsidiary reactions on the ^{87}Sr (1.33%) and ^{88}Sr (2.26%) impurities in the enriched ^{86}Sr target were estimated from the model calculation using the TALYS-1.9 code as described in Ref. [16] (see Table II). The calculated contributions were subtracted from the measured cross section of the radionuclide. For ^{82m}Rb

TABLE II. Corrections for the contributions of the deuteron-induced reactions on the impurities ^{87}Sr and ^{88}Sr present in the target material, deduced from the TALYS nuclear model calculations. A 5% systematic uncertainty was adopted for all correction factors.

Deuteron energy (MeV)	Laboratory	Contributions from ^{87}Sr and ^{88}Sr target isotopes (%)	
		^{84m}Rb	$^{84g+xm}$Rb
49.1 ± 0.3	FZJ[a]		7
47.9 ± 0.3			7
46.7 ± 0.3			8
45.5 ± 0.3			8
44.3 ± 0.3			9
43.0 ± 0.4			10
41.7 ± 0.4			11
40.4 ± 0.4			12
38.9 ± 0.4			14
36.2 ± 0.4			16
36.0 ± 0.4			17
33.1 ± 0.5			18
32.9 ± 0.5			18
30.1 ± 0.5			17
36.9 ± 0.3	LBNL	22	16
34.1 ± 0.3		26	18
31.1 ± 0.3		25	17
28.2 ± 0.3		24	16
28.1 ± 0.4		24	16
24.6 ± 0.4		20	13
21.7 ± 0.4		13	9
20.9 ± 0.4		11	8
18.5 ± 0.4		6	5
16.9 ± 0.4		3.4	3
15.2 ± 0.4		1.5	1.4
13.4 ± 0.5		0.4	0.4

[a]Irradiations were done at the CGR 930 Cyclotron in Louvain-la-Neuve but all other experimental work was done at FZJ.

and ^{83}Rb they were negligible, but for both the metastable state and the ground state of ^{84}Rb, they were significant. In both cases, the contributions increased with the increase in the deuteron energy, reaching maximum values of 26 and 18%, respectively, at around 34 MeV, and thereafter decreased with the increase in the deuteron energy.

The overall uncertainty in the cross section was obtained by summing in quadrature the individual uncertainties in: counting statistics (1–10%), efficiency of the detector (4%), γ-ray intensities (1–7%), half-life (0.1–0.2%), deuteron flux (6%), and sample homogeneity (up to 5%). The overall uncertainties of the measured cross sections are between 10 and 15% (1σ), including 5% systematic uncertainty in the estimation of the contribution of the subsidiary reactions deduced from the nuclear model calculations. The uncertainty in counting statistics for ^{84m}Rb ranged from 7 to 15%. Particularly for the two lowest deuteron energy points it was approximately 21%. The weak and poorly resolved peaks for this radionuclide are responsible for the large uncertainty in its counting statistics.

The uncertainty of the isomeric ratio was estimated from the individual uncertainties in counting statistics, detector efficiency, γ-ray intensity, and half-life of both the metastable state and the ground state. While dividing the formula for the cross sections of metastable state and ground state, the common parameters like flux of deuterons and weight of the sample were eliminated. The uncertainty in the isomeric cross-section ratio amounted to 9–12%, except for the two lowest-energy points where it was comparatively higher due to the large uncertainty associated in the peak area determination of the metastable state ^{84m}Rb.

Some thought was also given to possible interference through contributions from neutron-induced reactions. As is known, the breakup of intermediate-energy deuterons leads to the formation of energetic secondary neutrons which could induce threshold reactions like (n,xn), $(n,$charged particle), etc. In the present experiment on radionuclides of rubidium, the (n,xn) reactions had no significance because the target material ^{86}Sr was free of Rb. On the other hand, the $(n,$charged-particle) reactions, consisting of $(n,t)+(n,nd)+(n,p2n)$ on ^{86}Sr, could lead to ^{84}Rb, whose estimated cross section from the systematics of 53-MeV d/Be neutrons amounts to about 50 mb (millibarn) [27]. However, since the flux of the secondary neutrons incident on the ^{86}Sr sample is estimated to be only a few percent of all the generated neutrons, we conclude that the additional uncertainty in the cross section of ^{84}Rb due to the neutron effect should be <1%. For ^{83}Rb and ^{82m}Rb it should be even lower.

III. NUCLEAR MODEL CALCULATIONS

Three different approaches were used in the calculations. In two cases the TALYS-1.9 code was used for the calculation while in the third case the EMPIRE-3.2.3 code was used to simulate the cross sections.

In the first instance (marked as TALYS-a in figures), our approach involved optimizing certain crucial parameters of the model [20]. This included the ratio of the effective moment of inertia to the rigid-body moment of inertia parameter of the spin distribution of the level density ($\eta = \Theta_{\text{eff}}/\Theta_{\text{rig}}$ parameter). The calculations followed an iterative procedure (cf. Ref. [28]). We utilized a similar method for some other selected model parameters of the calculations, as described for the ^{86}Sr$(d,xn)^{87m,g,86m,g,85m,g}$Y reactions [16]. The code TALYS [29], version 1.9 was used to perform the calculations, employing an equidistant excitation energy grid. TALYS incorporates multiple nuclear models to analyze all significant nuclear reaction mechanisms within the 1-keV to 200-MeV energy range. The spherical optical model in the ECIS-06 code [30] was used to generate particle transmission coefficients with global parameters from Koning *et al.* [31] for neutrons and protons. For complex particles $(d,t,$ ^{3}He), the code employed a folding approach to construct the optical model parameters (OMPs) based on the neutron- and proton potential. Additionally, for alpha particles, the folding approach of TALYS was used instead of the default parameter set of Avrigeanu *et al.* [32] as it could be adjusted to the experimental data. The OMPs for deuteron, proton, and neutron were modified to achieve the best description of the

experimental data. Gamma-ray transmission coefficients were calculated using the energy-dependent gamma-ray strength function according to Kopecky and Uhl [33] for E1 radiation and according to Brink [34] and Axel [35] for other transition types. Preequilibrium reactions were modeled using the two-component exciton model in the TALYS code. The energy, spin, parity, and branching ratios for discrete levels were based on the RIPL-3 database [36]. In the continuum region, the level density was determined using the back-shifted Fermi gas model [37] with a slightly modified version for TALYS [31]. For η values, we relied on systematics developed by Sudár and Qaim [28]. It is important to note that the influence of discrete levels on the calculated isomeric cross-section ratio is highly significant. For several product nuclei, the properties of the low-lying levels and gamma transitions are not known well. To address this, many of the data are assumed and included in the TALYS input based on reference input parameter library (RIPL) [36]. In our previous works on protons and deuterons on ^{86}Sr target [20,16], we examined various options for the assumed properties of a few reaction products to reproduce reaction cross sections accurately. The level schemes employed in those works were also utilized in this study. It is in some way similar to the approach used in the creation of the TENDL library that attempts to fit the model parameters to the experimental data [38]. In this case, however, only a limited number of parameters of the TALYS code are used.

The second TALYS calculation (marked as TALYS-b in the figures) utilized the "best" input parameter values recommended for neutron-induced reaction on ^{86}Sr, including the use of the Fermi gas-level density model *(ldmodel 2)* and slightly modified (4%) values of the radial *(rvadjust)* and diffuseness *(avadjust)* parameters from the default Wood-Saxon potential form factor. In addition to these recommended values, the TALYS inputs were also altered to take into account recent results from Fox *et al.* on residual channel cross sections for protons up to 200 MeV on natural niobium [6] and arsenic targets [7], since these nuclei "bracket" the region near ^{86}Sr. Specifically, changes were made in the square of the preequilibrium exciton model scattering matrix elements. The changes include shifting the overall matrix element strength *(M2Constant)* as well as the energy-independent *(M2Limit)* and *(M2Shift)* values to 0.85, 2.5, and 0.9, relative to their default values of 1.0. Most relevantly for the (d,α) channel, the alpha-particle stripping cross section as described in the work by Kalbach [39] was doubled (e.g., *cstrip a 2.0*). Last, since the spins of the ^{84}Rb isomer and ground states differ significantly, the value of the spin cutoff parameter was halved and doubled relative to its default value (marked as TALYS-b with the relevant spin value). In both of these cases only nominal differences in the residual product cross sections were observed. Overall, the relative success of the TALYS model in reproducing the ^{84}Rb cross sections suggests that the preequilibrium adjustments seen in the papers by Fox *et al.* [6,7] may also be applicable to the results presented in this work.

The third calculation aimed to compare the TALYS results with another reaction model code which also emphasizes the direct processes, the isomeric cross sections, and the database of the input parameters. The selected code was EMPIRE-3.2.3 [40]. EMPIRE is also a modular system of nuclear reaction

codes, comprising various nuclear models, and designed for calculations over a broad range of energies and incident particles. The code accounts for the major nuclear reaction models, such as the optical model, coupled channels and DWBA (ECIS06 and OPTMAN), multi-step direct (ORION + TRISTAN), NVWY multistep compound, exciton model (PCROSS), hybrid Monte Carlo simulation, and the full-featured Hauser-Feshbach model including width fluctuations and the optical model for fission. A comprehensive library of input parameters based on the RIPL-3 library covers nuclear masses, optical model parameters, ground-state deformations, discrete levels and decay schemes, level densities, fission barriers, and γ-ray strength functions. The properly parametrized enhanced generalized superfluid model (EGSM) (including adjustment to discrete levels) is the default-level density formulation in the EMPIRE code; therefore, it is also referred to as "empire global specific model." The EGSM uses, as GSM, the superfluid model below critical excitation energy and the Fermi gas model above. Enhancement compared to GSM relates mainly to the spin distribution in the Fermi gas model.

During the calculation, the EMPIRE-specific level densities were selected. Exciton model calculations were performed with the PCROSS code. Cluster emission utilized parametrization of the Iwamoto-Harada model. The mean-free path parameter in PCROSS was set to the recommended 1.5 value. Gamma emission width is not normalized. Optical model parameters for neutron, proton, alpha, deuteron, triton, and ^{3}He used the RIPL catalog numbers 1429 [41], 5405 [42], 9600 [42], 6200 [43], 7100 [44], and 8100 [44], respectively. For deuteron breakup parametrization, the Kalbach model was used and the stripping cross section for (d,n) was calculated by using the transfer cross sections, normalized to the reaction cross section multiplied by a factor of 0.9. For each product nuclide, two calculations were carried out: EMPIRE def, using default parameters, and EMPIRE LevSch, in which the same level scheme was used as in TALYS-a.

IV. RESULTS AND DISCUSSION

A. Reaction cross sections

The measured cross sections for the reactions ^{86}Sr$(d,x)^{84m}$Rb, ^{86}Sr$(d,x)^{84g+xm}$Rb, ^{86}Sr$(d,x)^{83}$Rb, ^{86}Sr$(d,x)^{83}$Rb(cum), and ^{86}Sr$(d,x)^{82m}$Rb are given in Table III, together with the estimated uncertainties. The cross section for ^{83}Rb refers to its independent production through the ^{86}Sr$(d,x)^{83}$Rb reaction, whereas the cross-section ^{83}Rb(cum) denotes the sum of its independent formation and the contribution via the decay of ^{83}Sr and ^{83}Y. In the case of ^{84}Rb, the contributions to its production from the subsidiary reactions on the impurities ^{87}Sr and ^{88}Sr present in the enriched target ^{86}Sr were subtracted. All data reported here have been measured.

B. Excitation functions

1. ^{86}Sr$(d,x)^{84m}$Rb and ^{86}Sr$(d,x)^{84g+xm}$Rb reactions

The isotope ^{84}Rb has two isomeric states: the short-lived metastable state ^{84m}Rb ($T_{1/2} = 20.26$ min) and the relatively long-lived ^{84g}Rb ($T_{1/2} = 32.82$ d). It should be mentioned that
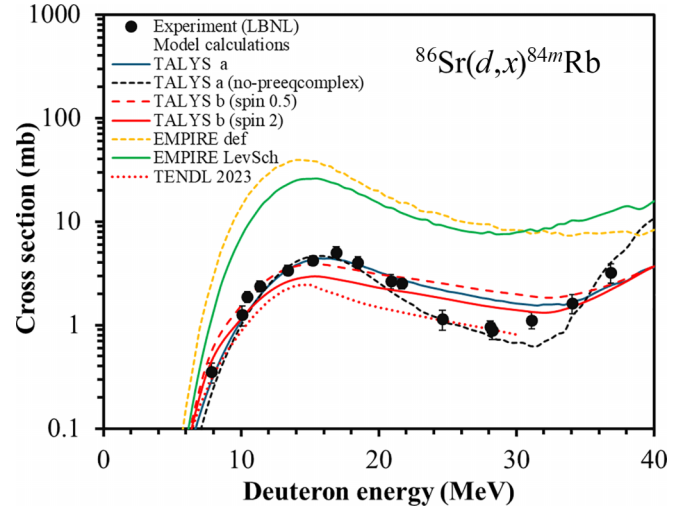

FIG. 1. Comparison of experimental data with results of calculations done using five versions of TALYS (a), with optimized parameters and without Kalbach model; (b) with spins 0.5 and 2.0; TENDL-2023) and two versions of EMPIRE (def and LevSch) for the ^{86}Sr$(d,x)^{84m}$Rb reaction.

the measured data are for the cumulative production of the ground-state ^{86}Sr$(d,x)^{84g+xm}$Rb and the direct formation of the metastable state ^{86}Sr$(d,x)^{84m}$Rb. To make them comparable to the value in this experiment the ^{86}Sr$(d,x)^{84g+xm}$Rb data were calculated using the formula $\sigma_{g+xm} = (\sigma_g + P_m \frac{\lambda_m}{\lambda_m - \lambda_g} \sigma_m)$ [19], where P_m is the probability of the isomeric transition to the ground state, and the factor x describes the correction for the direct decay of the metastable state to ^{84}Kr. It is negligible here because ^{84m}Rb decays 100% by isomeric transition (IT) to ^{84g}Rb.

Figure 1 depicts the measured excitation function of the ^{86}Sr$(d,x)^{84m}$Rb reaction. The results are, however, limited to 37 MeV because in the FZJ experiment, the short-lived product could not be measured since it decayed out during the transport from Louvain-la-Neuve to the counting laboratory in Jülich. As seen in Fig. 1, the cross section rises sharply with the increase in the deuteron energy, reaching the maximum value of 5.1 ± 0.7 mb at 16.9 MeV, and thereafter, the decreasing trend continued up to incident energy of 30 MeV. This shape is attributed to the ^{86}Sr$(d,\alpha)^{84m}$Rb reaction. At energies beyond 30 MeV, the cross section increases again due to the opening of channels for the formation of ^{84m}Rb, i.e., multinucleon emissions in the higher-energy region. Comparing the results of calculations using the codes TALYS and EMPIRE, the TALYS results are consistent with the experimental data in both shape and magnitude, whereas the EMPIRE values agree with the experiment in shape but are overestimated in magnitude. In EMPIRE-LevSch, the same level scheme was used as in TALYS-a calculation; in those cases, the shape of the calculation seems better. The figure also shows the TENDL library data [38] for this reaction, which, however, are given only up to 30 MeV. Since no earlier experimental data for the ^{86}Sr$(d,\alpha)^{84m}$Rb reaction were available, the TENDL evaluation contains only TALYS calculation with the default parameters. We also plot the TALYS-a calculation with-

TABLE III. Measured cross sections for the production of radionuclides via ^{86}Sr +d reactions.

Deuteron energy (MeV)	Laboratory	Measured cross sections of the activation products (mb)				
		^{84m}Rb	^{84}Rb(cum)[a]	^{83}Rb	^{83}Rb(cum)[b]	^{82m}Rb
49.1 ± 0.3	FZJ		35 ± 3.9	30 ± 4	69 ± 9	35 ± 5
47.9 ± 0.3			33 ± 3.6	27 ± 3	52 ± 6	37 ± 5
46.7 ± 0.3			34 ± 3.7	29 ± 4	49 ± 6	47 ± 5
45.5 ± 0.3			30 ± 3.2	26 ± 3	38 ± 5	52 ± 5
44.3 ± 0.3			27 ± 3.0	26 ± 3	34 ± 4	55 ± 5
43.0 ± 0.4			20 ± 2.2	22 ± 3	26 ± 3	57 ± 5
41.7 ± 0.4			15 ± 1.7	21 ± 3	23 ± 3	58 ± 5
40.4 ± 0.4			15 ± 1.6	25 ± 3	27 ± 3	61 ± 8
38.9 ± 0.4			11 ± 1.0	24 ± 3	25 ± 3	63 ± 8
36.2 ± 0.4			8.6 ± 1.0	29 ± 4	30 ± 4	61 ± 8
36.0 ± 0.4			8.3 ± 0.9	30 ± 4	30 ± 4	61 ± 7
33.1 ± 0.5			7.1 ± 0.8	40 ± 5	40 ± 5	50 ± 8
32.9 ± 0.5			7.2 ± 0.8	41 ± 5	41 ± 5	42 ± 6
30.1 ± 0.5			6.1 ± 0.7	45 ± 6	45 ± 6	25 ± 3
36.9 ± 0.3	LBNL	3.2 ± 0.7	9.5 ± 1.0	28 ± 4	28 ± 4	
34.1 ± 0.3		1.6 ± 0.3	6.4 ± 0.7	37 ± 5	37 ± 5	
31.1 ± 0.3		1.1 ± 0.2	5.6 ± 0.6	40 ± 5	40 ± 5	29 ± 4.4
28.2 ± 0.3		0.9 ± 0.2	4.5 ± 0.5	41 ± 5	41 ± 5	10.0 ± 1.5
28.1 ± 0.4		1.0 ± 0.1	4.8 ± 0.5	41 ± 6	41 ± 6	8.0 ± 0.9
24.6 ± 0.4		1.2 ± 0.3	4.8 ± 0.5	46 ± 6	46 ± 6	
21.7 ± 0.4		2.5 ± 0.3	7.5 ± 0.8	28 ± 4	28 ± 4	
20.9 ± 0.4		2.7 ± 0.4	7.3 ± 0.8	27 ± 3	27 ± 3	
18.5 ± 0.4		4.0 ± 0.5	9.7 ± 1.0	18 ± 2	18 ± 2	
16.9 ± 0.4		5.1 ± 0.7	13.7 ± 1.4	16 ± 2	16 ± 2	
15.2 ± 0.4		4.3 ± 0.4	12.2 ± 1.3	5 ± 0.6	5 ± 0.6	
13.4 ± 0.5		3.4 ± 0.4	11.9 ± 1.3	2.5 ± 0.3	2.5 ± 0.3	
11.4 ± 0.5		2.4 ± 0.3	10.2 ± 1.1	0.5 ± 0.1	0.5 ± 0.1	
10.5 ± 0.5		1.9 ± 0.2	9.4 ± 1.1			
10.1 ± 0.5		1.3 ± 0.3	6.7 ± 0.7			
7.9 ± 0.5		0.35 ± 0.1	2.1 ± 0.2			
6.2 ± 0.5			1.1 ± 0.1			

[a]Cumulative cross section of this product describes the sum of its independent formation and via the decay of the metastable state.
[b]Cumulative cross section of this product describes the sum of its independent formation and via the decay of the radionuclides ^{83}Sr and ^{83}Y.

out using the Kalbach model [39] for pickup, stripping, and knockout reactions, in addition to the exciton model, in the preequilibrium region. It is marked by "no preeqcomplex." Except for some lower cross-section values over the deuteron energy range of 20 to 35 MeV, the results are in agreement with the other TALYS calculations.

Figure 2 shows the excitation function of the ^{86}Sr$(d,x)^{84g+xm}$Rb reaction and consists of measurements done at both LBNL and FZJ up to 49 MeV. The results of nuclear model calculations, based on the codes TALYS and EMPIRE, are also shown in Fig. 2. Whereas the TALYS data agree fairly well with the experimental values, the EMPIRE results are by about an order of magnitude higher. The figure also shows the TENDL library data for this reaction, but they are limited only up to 30 MeV. The good shapes but very high values of EMPIRE for both ^{84m}Rb and $^{84g+xm}$Rb suggest that issues are more related to calculation of transmission coefficients than the angular momentum.

It should be pointed out that the production cross section of the radionuclide ^{84}Rb measured by the activation method contains contributions from several different routes. The most
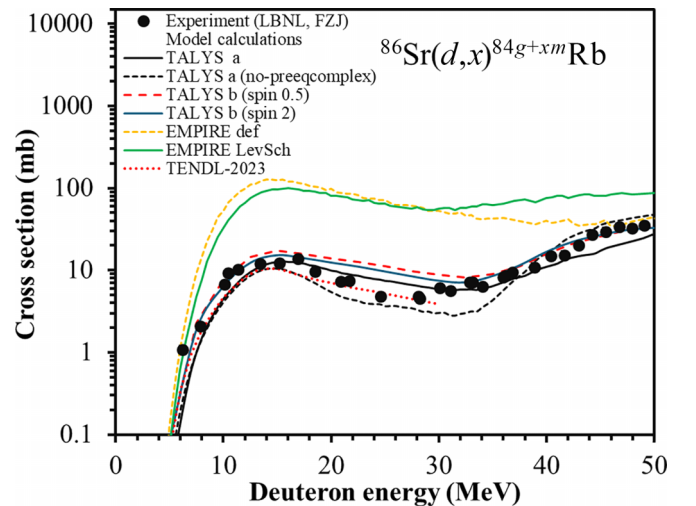

FIG. 2. Comparison of experimental data with results of calculations done using five versions of TALYS (see text) and two versions of EMPIRE (def and LevSch) for the ^{86}Sr$(d,\alpha)^{84g+xm}$Rb reaction.
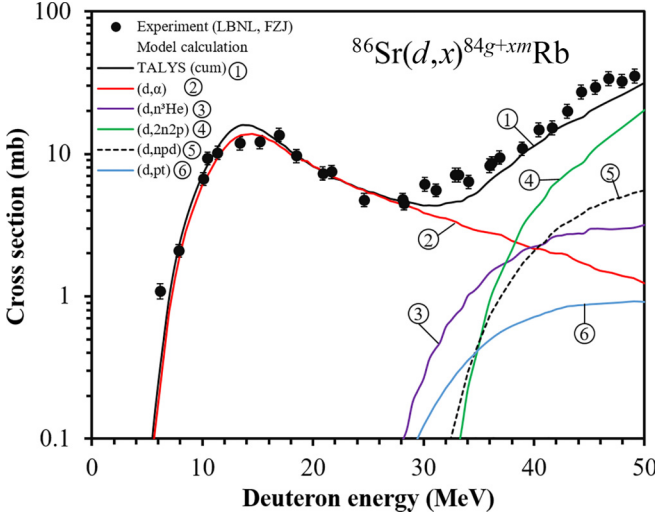
FIG. 3. Modified version of Fig. 2 showing the individual contributions of α emission and four other reactions to the formation of ^{84}Rb in deuterons on ^{86}Sr in the TALYS calculation without using the Kalbach model [39].

important reaction type is the (d,α) which includes direct, compound, exciton model, precompound nucleon transfer, and knockout contributions. A more detailed breakdown of the TALYS calculations for various contributing channels is given in Fig. 3 and shows that the product ^{84}Rb is formed almost exclusively via the ^{86}Sr$(d,\alpha)^{84}$Rb reaction up to about 25-MeV deuteron energy. Beyond that energy, the thresholds of many of the multinucleon emission reactions (e.g., n^3He, $2n2p$, npd, pt, etc.) open up and their contributions, in comparison to a bound α-particle where emission starts increasing, becoming dominant at the maximum energy of 49 MeV investigated in this work. The cross sections of the $(d,n^3$He$)$ and (d,pt) reactions are appreciably smaller than those of the multinucleon emission processes.

2. ^{86}Sr$(d,x)^{83}$Rb reaction

For ^{83}Rb the cumulative cross section includes the decay of the coproduced ^{83}Sr and ^{83}Y. These decay processes play a role both during and after the irradiation. The general solution is ordered as the sum of different half-life components. In the cumulative case, all short half-life components become negligible, and the cumulative cross section can be read from the multiplier of the long-lived component. For details see Ref. [45], modifying the equation for this case in the following form (the decay ratio for the level scheme is also needed):
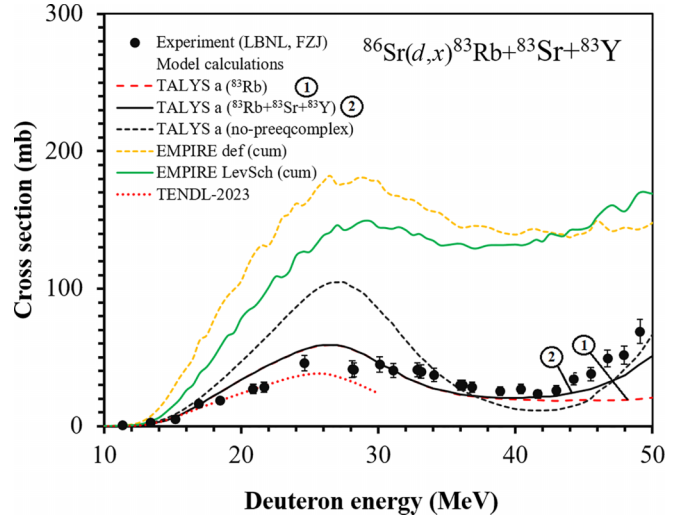
$$\sigma_{\text{cum}} = \left(\sigma_{83\text{Rb}} + P_{83m\text{Sr}} \overset{\text{decay}}{\to}\, {}_{83}\text{Rb} \frac{\lambda_{83}\text{Sr}}{\lambda_{83}\text{Sr} - \lambda_{83}\text{Rb}} \left(\sigma_{83g\text{Sr}} + P_{83m\text{Sr}} \overset{\text{decay}}{\to}\, {}_{83g}\text{Sr} \frac{\lambda_{83m}\text{Sr}}{\lambda_{83m}\text{Sr} - \lambda_{83g}\text{Sr}} (\sigma_{83g\text{Sr}} + C1_{83Y}) + C2_{83Y} \right) \right), \quad (1)$$

the $C1_{83Y}$ and $C2_{83Y}$ are the decay contributions of the ^{83}Y to ^{83m,g}Sr. We have calculated these too, but their contribution is practically negligible, i.e., the calculated cross sections are very small, yet our calculation includes them.

The cumulative cross sections for the formation of ^{83}Rb, i.e., directly via the reaction ^{86}Sr$(d,x)^{83}$Rb and from the decay of ^{83}Sr and ^{83}Y, are shown in Fig. 4, together with the results of model calculations based on three versions of the code TALYS and two versions of EMPIRE (def and Levsch). The experimental cross-section data for the independent formation of ^{83}Rb, mainly via the ^{86}Sr$(d,n\alpha)$ reaction, [i.e., after subtracting the decay contributions from ^{83}Sr and ^{83}Y using the formula (1)] are also shown in Fig. 4, together with the corresponding results of the model calculation.

The EMPIRE calculational results are very far from the experimental cumulative data of ^{83}Rb. On the other hand, the TALYS calculation describes the cumulative cross section very well up to about 42 MeV but slightly underestimates it above 44 MeV. Regarding the independent formation cross section of ^{83}Rb, the TALYS calculation for the ^{86}Sr$(d,n\alpha)^{83}$Rb channel is close to the experimental data. However, above 44 MeV the calculated excitation function is lower than the experimental data. The figure shows also the data of the TENDL library up to 30 MeV. It agrees with our calculation up to about 20-MeV deuteron energy but at higher energy it is lower than our calculation for the ^{86}Sr$(d,n\alpha)^{83}$Rb cross section. The calculated cross sections without the Kalbach model give significantly higher data below 37-MeV deuteron energy than our final calculation.

FIG. 4. Comparison of experimental data with the results of model calculations for the cumulative ^{86}Sr$(d,x)^{83}$Rb $+ {}^{83}$Sr $+ {}^{83}$Y process as black curve (2) as well as the independent ^{86}Sr$(d,n\alpha)^{83}$Rb reaction as red dashed curve (1). The experimental (d,x) process is denoted by black points.

3. ^{86}Sr$(d,x)^{82m}$Rb reaction

This radionuclide is formed only independently because ^{82}Sr, also formed in the irradiation, decays 100% to the short-lived ground-state ^{82}Rb ($T_{1/2} = 1.3$ min). The excitation
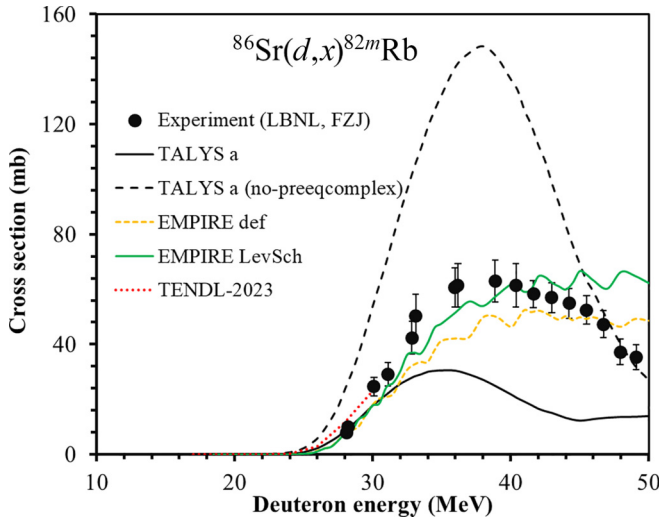
FIG. 5. Comparison of experimental data with the model calculations based on three versions of the code TALYS and two versions of the code EMPIRE for the $^{86}Sr(d,x)^{82m}Rb$ reaction.
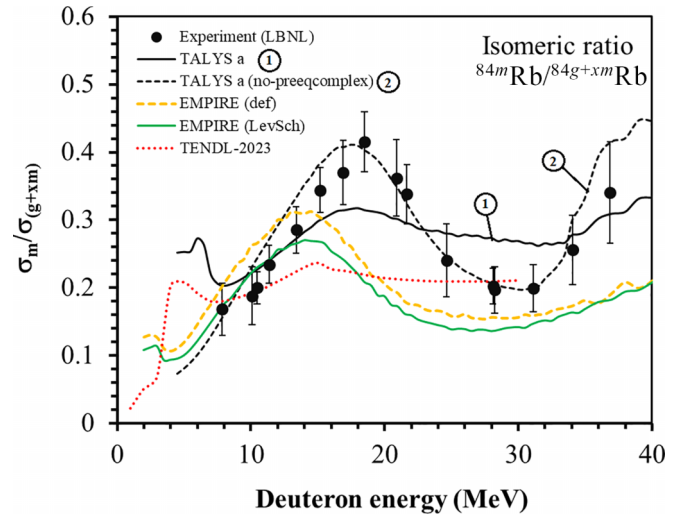

FIG. 6. Comparison of experimental data with the results of model calculations done using three versions of TALYS (see text) and two versions of EMPIRE (def and LevSch) for the isomeric cross-section ratios of the $^{86}Sr(d,x)^{84m}Rb$ and $^{86}Sr(d,x)^{84g+xm}Rb$ reactions. Plotted are σ_m/σ_{g+xm} values against the deuteron energy.

function is shown in Fig. 5. The calculations with TALYS were performed with and without the Kalbach model and the contribution of the $(d,\alpha 2n)$ reaction channel was also determined. The TENDL library has data only below 30 MeV and this range agrees quite well with the present calculation. The experimental data are quite close to the model below 32 MeV, but above this energy, the model calculation is much below the experimental data. The calculation without the Kalbach model is considerably higher than the experimental data; with proper adjustment of the complex particle emission a better agreement could be obtained, but as described in the next section, this is questionable, because here only isomeric cross sections were measured. The calculated cross section of the reaction channel $(d,\alpha 2n)$ falls exactly on the TALYS calculation; therefore, the contribution of the multinucleon emission seems negligible. This follows from the higher thresholds of those reaction channels too. The EMPIRE calculation results are nearer to the experimental data than the TALYS results.

C. Isomeric cross-section ratios

The measured isomeric cross-section ratios of the $^{86}Sr(d,x)^{84m}Rb$ and $^{86}Sr(d,x)^{84g+xm}Rb$ reactions are shown in Fig. 6. The initial increase in the ratio with the increase in the deuteron energy is attributed to the higher spin of the metastable state (6^-) as compared to that of the ground state (2^-). Beyond 18 MeV, the ratio decreases up to 30 MeV, but above 32 MeV it increases again with the increase of deuteron energy, presumably due to higher contributions of multinucleon emission reactions in the formation of higher spin of the metastable state (6^-) than those to the low-spin (2^-) ground state. The results of nuclear model calculations based on the code TALYS with three versions, and EMPIRE with two versions are also shown in Fig. 6. In general, the TALYS code describes the experimental data better than both versions of EMPIRE . On the other hand, the TALYS results underestimate the experimental data around 18 MeV and overestimate in

the energy range of 28 to 32 MeV. The figure shows also the data of the TENDL library which have similar behavior to our calculation, but somewhat lower values.

The figure depicts also the calculation without the Kalbach model contribution. This curve describes the experimental data fairly well but shows rather large deviation from the experiment in the low excitation energy range. This deviation may come from a deficient knowledge of the level scheme of ^{84}Rb.

A similar behavior appears to occur when the multinucleon emission starts above 30 MeV. The η value for the best description of the isomeric cross-section ratios was found to be 1.15 ± 0.08. This fits well in the systematics described in Ref. [28].

The preequilibrium processes can describe the full cross section, but they are not able to calculate their contributions to the discrete levels of the nucleus. The standard method uses the preequilibrium spin distribution to equal the relative spin-dependent population after the emission from the compound nucleus. It seems that this does not apply to the contribution of the Kalbach model. It is shown in Fig. 2 that the calculation with the Kalbach model describes the $^{86}Sr(d,x)^{84g+xm}Rb$ reaction cross section fairly well; therefore, the contribution of the Kalbach model to the isomer production appears to be incorrect. We, therefore, did not aim to change the model parameters for the $^{86}Sr(d,x)^{82m}Rb$ reaction.

V. CONCLUDING REMARKS

We measured cross sections for the formation of several radionuclides in the interactions of deuterons of energies up to 49 MeV with an enriched ^{86}Sr target using the activation technique. Nuclear model calculations using the codes TALYS 1.9 and EMPIRE 3.2.3 were performed and the results were compared with the

experimental data to test the validity of those calculational codes. The results on (d,xn) reactions leading to the formation of ^{87m,g}Y, ^{86m,g}Y, and ^{85m,g}Y were reported earlier [16]; they showed that the (d,n) reaction cross sections are not described satisfactorily by both the codes, possibly due to inadequacy in the description of the deuteron breakup process. For the $(d,2n)$ and $(d,3n)$ reactions, however, the TALYS code described both the excitation functions and isomeric cross-section ratios with partial success. The results on (d,x) reactions leading to the formation of ^{84m,g}Rb, ^{83}Rb, and ^{82m}Rb, reported in this paper, show that the code EMPIRE predicts much higher values than the code TALYS. Except for ^{82m}Rb, fairly good agreement is obtained between the experimental data and the TALYS calculation, provided a careful choice of the input model parameters is done. It came to light that the Kalbach model contribution to isomeric-state production seems incorrect in the TALYS calculations. Furthermore, some information could also be deduced on competition between the emission of multinucleons and a bound α particle. Beyond its energy threshold, with the increasing deuteron energy, the multinucleon emission process contributes increasingly more so to the product formation than the emission of a complex particle. We have attempted to show that the summed contribution of the (n,t), (n,dn), and $(n,p2n)$ reactions on ^{86}Sr to the formation of ^{84}Rb through breakup neutrons could amount up to 1%.

A further point worth mentioning is the possibility of the use of the data in developing alternative production routes of ^{82m}Rb, and ^{83}Rb using the deuteron beam. The radionuclide ^{82m}Rb ($T_{1/2} = 6.47$ h) has been suggested for myocardial perfusion study via PET [17], as a substitute for the very short-lived ^{82}Rb ($T_{1/2} = 1.3$ min), which is obtained via a ^{82}Sr $/^{82}$Rb generator system [3–5]. The radionuclide ^{83}Rb ($T_{1/2} = 86.2$ d), on the other hand, is a potential candidate for Auger therapy (cf. Ref. [18]), because it decays 100% by electron capture (EC) and emits many low-energy electrons. The optimum energy ranges for the production of those two radionuclides using deuterons could be deduced from the cross-section data gained in this investigation.

After publication, the cross-section data are compiled by national and regional nuclear data centers and placed in the international experimental data file (EXFOR), managed by the IAEA.

[1] Experimental Nuclear Reaction Data (EXFOR), Database version of 2024-06-25, Retrieved from IAEA NDS website 2024.

[2] S. M. Qaim, *Medical Radionuclide Production-Science and Technology* (De Gruyter, Berlin/Boston, 2019).

[3] S. M. Qaim, Radiochim. Acta **100**, 635 (2012).

[4] S. M. Qaim, Nucl. Med. Biol. **44**, 31 (2017).

[5] S. M. Qaim, B. Scholten, I. Spahn, and B. Neumaier, Radiochim. Acta **107**, 1011 (2019).

[6] M. B. Fox, A. S. Voyles, J. T. Morrell, L. A. Bernstein, A. M. Lewis, A. J. Koning, J. C. Batchelder, E. R. Birnbaum, C. S. Cutler, D. G. Medvedev, F. M. Nortier, E. M. O'Brien, C. Vermeulen *et al.*, Phys. Rev. C **103**, 034601 (2021).

[7] M. B. Fox, A. S. Voyles, J. T. Morrell, L. A. Bernstein, J. C. Batchelder, E. R. Birnbaum, C. S. Cutler, A. J. Koning, A. M. Lewis *et al.*, Phys. Rev. C **104**, 064615 (2021).

[8] N. Amjed, M. N. Aslam, M. Hussain, and S. M. Qaim, Radiochim. Acta **109**, 525 (2021).

[9] S. M. Qaim, J. Radioanal. Nucl. Chem. **333**, 3577 (2024).

[10] S. M. Qaim, I. Spahn, B. Scholten, and B. Neumaier, Radiochim. Acta **104**, 601 (2016).

[11] P. Bém, E. Šimečková, M. Honusek, U. Fischer, S. P. Simakov, R. A. Forrest, M. Avrigeanu, A. C. Obreja, F. L. Roman, and V. Avrigeanu, Phys. Rev. C **79**, 044610 (2009).

[12] M. Avrigeanu, E. Šimečková, U. Fischer, J. Mrázek, J. Novak, M. Štefánik, C. Costache, and V. Avrigeanu, Phys. Rev. C **94**, 014606 (2016).

[13] A. Kreisel, L. Weissman, A. Cohen, T. Hirsh, A. Shor, O. Aviv, I. Eliyahu, M. Avrigeanu, and V. Avrigeanu, Phys. Rev. C **99**, 034611 (2019).

[14] A. Guertin, E. Nigron, M. Sitarz, C. Duchemin, F. Haddad, and V. Métivier, in *Proceedings of the 15th International Conference on Nuclear Reaction Mechanisms*, edited by F. Cerutti, A. Ferrari, T. Kawano, F. Salvat-Pujol, and P. Talou (CERN, Varenna, Italy, 2018), pp. 355–360.

[15] M. S. Uddin, M. S. Basunia, and S. M. Qaim, Radiochim. Acta **109**, 727 (2021).

[16] M. S. Uddin, S. Sudár, M. S. Basunia, B. Scholten, S. Spellerberg, A. S. Voyles, J. T. Morrell, I. Spahn, A. Hermanne, L. A. Bernstein, B. Neumaier, and S. M. Qaim, Eur. Phys. J. A **60**, 128 (2024).

[17] Z. Kovács, F. Tárkányi, S. M. Qaim, and G. Stöcklin, Appl. Radiat. Isot. **42**, 831 (1991).

[18] M. S. Uddin, M. S. Basunia, I. Spahn, S. Spellerberg, R. Khan, M. M. Uddin, L. A. Bernstein, B. Neumaier, and S. M. Qaim, Radiochim. Acta **111**, 81 (2023).

[19] M. S. Uddin, B. Scholten, M. S. Basunia, S. Sudár, S. Spellerberg, A. S. Voyles, H. Zaneb, J. T. Morrell, J. Rios, I. Spahn, L. A. Bernstein, B. Neumaier, and S. M. Qaim, Radiochim. Acta **108**, 747 (2020).

[20] M. S. Uddin, M. S. Basunia, S. Sudár, B. Scholten, S. Spellerberg, A. S. Voyles, J. T. Morrell, M. B. Fox, I. Spahn, O. Felden, R. Gebel, L. A. Bernstein, B. Neumaier, and S. M. Qaim, Eur. Phys. J. A **58**, 67 (2022).

[21] J. Fitzgerald, JF Computing Services, Oxfordshire, SN7 8LE United Kingdom, https://www.jimfitz.co.uk/ (last updated 8 October 2018).

[22] J. K. Tuli, Nuclear Data Sheets **81**, 331 (1997).

[23] J. K. Tuli and E. Browne, Nucl. Data Sheets **157**, 260 (2019).

[24] E. A. McCutchan, Nucl. Data Sheets **125**, 201 (2015).

[25] D. Abriola, M. Bostan, S. Erturk, M. Fadil, M. Galan, S. Juutinen, T. Kibédi, F. Kondev, A. Luca, A. Negret, N. Nica, B. Pfeiffer, B. Singh, A. Sonzogni, J. Timar, J. Tuli, T. Venkova, and K. Zuber, Nucl. Data Sheets **110**, 2815 (2009).

[26] A. Hermanne, A. V. Ignatyuk, R. Capote, B. V. Carlson, J. W. Engle, M. A. Kellett, T. Kibédi, G. Kim, F. G. Kondev, M. Hussain, O. Lebeda, A. Luca, Y. Nagai, H. Naik, A. L. Nichols, F. M. Nortier, S. V. Suryanarayana, S. Takács, F. Tárkányi, and M. Verpelli, Nucl. Data Sheets **148**, 338 (2018).

[27] S. M. Qaim and R. Wölfle, Nucl. Phys. A **295**, 150 (1978).

[28] S. Sudár and S. M. Qaim, Nucl. Phys. A. **979**, 113 (2018).

[29] A. J. Koning, S. Hilaire, and M. C. Duijvestijn, in *Proceedings of the International Conference on Nuclear Data for Science and Technology, April 22–27, 2007* (EDP Sciences, Nice, France, 2007), pp. 211–214.

[30] J. Raynal, Notes on ECIS94, CEA Saclay Reports, CEA-N-2772, 1994.

[31] A. J. Koning, S. Hilarie, and S. Goriely, Nucl. Phys. A **810**, 13 (2008).

[32] V. Avrigeanu, M. Avrigeanu, and C. Mănăilescu, Phys. Rev. C **90**, 044612 (2014).

[33] J. Kopecky and M. Uhl, Phys. Rev. C **41**, 1941 (1990).

[34] D. M. Brink, Nucl. Phys. **4**, 215 (1957).

[35] P. Axel, Phys. Rev. **126**, 671 (1962).

[36] R. Capote, M. Herman, P. Oblozinsky, P. Young, S. Goriely, T. Belgya, A. Ignatyuk, A. J. Koning, S. Hilaire, V. Plujko, M. Avrigeanu, O. B. M. Chadwick, T. Fukahori, S. Kailas, J. Kopecky, V. Maslov, G. Reffo, M. Sin, E. Soukhovitskii, P. Talou, H. Yinlu, and G. Zhigang, Nucl. Data Sheets **110**, 3107 (2009).

[37] Dilg, W. Schantl, H. Vonach, and M. Uhl, Nucl. Phys. A **217**, 269 (1973).

[38] A. J. Koning, D. Rochman, J. Ch. Sublet, N. Dzysiuk, M. Fleming, and S. van der Marck, Nucl. Data Sheets **155**, 1 (2019).

[39] C. Kalbach, Phys. Rev. C **71**, 034606 (2005).

[40] M. Herman, R. Capote, B. V. Carlson, P. Oblozinsky, M. Sin, A. Trkov, H. Wienke, and V. Zerkin, Nucl. Data Sheets **108**, 2655 (2007).

[41] A. J. Koning and J. P. Delaroche, Nucl. Phys. A **713**, 231 (2003).

[42] V. Avrigeanu, P. E. Hodgson, and M. Avrigeanu, Report OUNP-94-02 (1994); Phys. Rev. C **49**, 2136 (1994).

[43] H. An and C. Cai, Phys. Rev. C **73**, 054605 (2006).

[44] F. D. Becchetti, Jr. and G. W. Greenlees, Phys. Rev. **182**, 1190 (1969).

[45] S. M. Qaim, S. Sudár, B. Scholten, A. J. Koning, and H. H. Coenen, Appl. Radiat. Isotopes **85**, 101 (2014).